Endoscopic sensing of distal lung physiology

IOP Conf. Series: Journal of Physics: Conf. Series 1151 (2019) 012009 doi:10.1088/1742-6596/1151/1/012009

Endoscopic sensing of distal lung physiology

Debaditya Choudhury*[1,2†], Michael G Tanner[1,2†], Sarah McAughtrie[3], Fei Yu[4], Bethany Mills[2], Tushar R Choudhary[2], Sohan Seth[5], Thomas H Craven[2], James M Stone[4], Ioulia K Mati[3], Colin J Campbell[3], Mark Bradley[2,3], Christopher K I Williams[5], Kevin Dhaliwal[2], Timothy A Birks[4], Robert R Thomson[1,2]

[1]Institute of Photonics and Quantum Sciences, Heriot-Watt University, Edinburgh UK.
[2]EPSRC IRC Hub, MRC Centre for Inflammation Research, Queen's Medical Research Institute (QMRI), University of Edinburgh, Edinburgh UK.
[3]School of Chemistry, University of Edinburgh, Edinburgh UK.
[4]Centre for Photonics and Photonic Materials, Department of Physics, University of Bath, Bath UK
[5]School of Informatics, University of Edinburgh, Edinburgh UK.
[†]*Contributed equally*

[*]Email: D.Choudhury@hw.ac.uk

Abstract. The alveolar space forms the distal end of the respiratory tract where chemoreceptor driven gas exchange processes occur. In healthy humans, the physiological state within the alveoli is tightly regulated by normal homeostatic mechanisms. However, pulmonary abnormalities such as chronic obstructive pulmonary disease may induce significant perturbation of the homeostatic baselines of physiology as well as cause host tissue damage. Therefore, physiological parameters (pH, glucose, oxygen tension) within the alveolar space provide a key biomarker of innate defence. Here, we discuss an endoscope-deployable fibre-optic optrode for sensing pH in the alveolar space. In order to circumvent the unwanted Raman signal generated within the fibre, the optrode consists of a custom asymmetric dual-core optical fibre designed for spatially separated optical pump delivery and SERS signal collection. pH sensing is achieved using the surface enhanced Raman spectroscopy (SERS) signal generated from functionalised gold nanoshell sensors. We show a ~ 100-fold increase in SERS signal-to-fibre background ratio and demonstrate multiple site pH sensing in the alveoli of an ex vivo ovine lung model with a measurement accuracy of ± 0.07 pH unit.

1. Introduction

The complex synergism between the homeostatic mechanisms in the human body rigorously maintains a physiologically optimal acid-base balance by regulating the ratio of the dissolved carbon dioxide and bicarbonate ions in the extra-cellular fluid (ECF). Inflammatory lung diseases such as pneumonia can drastically perturb the homeostatic baseline of physiology in the alveoli. Furthermore, in pulmonary disease conditions such as chronic obstructive pulmonary disorder, the homeostatic baselines of physiology may be significantly off-set. Existing patient monitoring technology does not incorporate *in situ* sensing in the distal lung ECF. There are established aspiration procedures such as bronchoalveolar lavage (BAL) and bronchoscopic transbronchial lung biopsy that allow pre-instilled saline fluid and tissue samples to be retrieved from the diseased anatomic subsegments in the lung. However, such

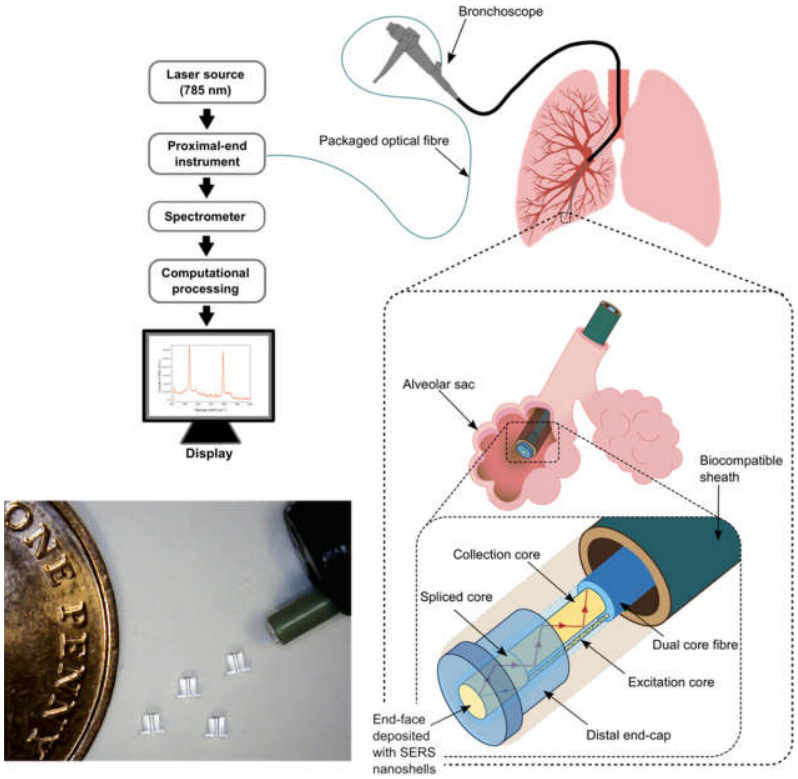

Figure 1. Schematic illustration of the fibre-optic sensing system and the miniaturized optrode for measuring alveolar pH (First published in [1]).

procedures are not suitable for bedside monitoring and aspirate samples are ordinarily examined *in vitro* using cytologic and histochemical methods. Moreover, the pH of post-aspirated BAL fluid is not representative of the pH of the endogenous and epithelial lining fluids within the alveolar environment due to the intrusive nature of the aspiration process and uncertainties associated with the aspirate volume, its dilution and temperature. Therefore, the prospect for a bedside instrument that permits the minimally invasive, bedside monitoring of pH in the distal lung of critically ill ventilated patients *in vivo* is an unmet clinical need.

Here, we discuss the development of a bronchoscope-deployable SERS based fibre-optic pH sensing probe that features a custom design to circumvent the strong Raman background generated within the fibre. We further discuss the experimental validation of the probe in an *ex vivo* ovine lung model.

2. Probe design and experimental methodology

The benefit of using SERS as an analytical technique is underpinned by the ability to detect plasmonically enhanced spectral signatures from Raman-active analytes with exceptional sensitivity and specificity. The SERS nanosensors must be incorporated at the distal end of a fibre-optic device to allow *in vivo* application. This has been the subject of extensive research and several reports are available demonstrating fibre-optic sensing schemes and distal tip-engineered surfaces activated with SERS nanosensors [2-4]. The most common design incorporates a single fibre to deliver the coherent excitation light to the nanosensors as well as collect the incoherent Raman-shifted light for spectral analysis. The fundamental problem with this approach is that the SERS signals of interest are swamped by the presence of strong, broadband Raman light in the low wavenumber region ($\leq$ 2000 cm^{-1}) [5] that originates within the fibre itself. Several probe designs to circumvent this drawback have been investigated [6-13], which typically involve the use of additional fibres positioned appropriately to

ensure adequate collection efficiency while reducing the fibre background. However, the large lateral dimensions of such instruments preclude their use in the distal lung (alveoli) and other anatomical sites where miniaturisation is essential for access and safety [3, 14].

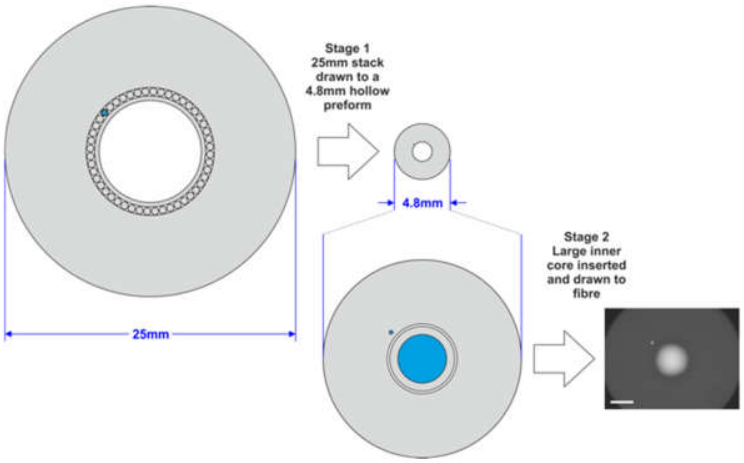

Figure 2. Schematic diagram showing the custom asymmetric dual-core fibre (First published in [1]). Scale bar is 20 μm

Here we used a single multicore fibre optrode that features an asymmetric core geometry to allow the fibre Raman background to be suppressed during data acquisition. We fabricated a custom-drawn 3 m long dual-core optical fibre with graded-index Ge:doped cores of size 4.4 μm and 28 μm. The fibre was fabricated in two stages using a modification to the stack-and-draw method developed to make photonic crystal fibres [15]. The 4.4 μm core was designed to support a single-mode (SM) at the excitation wavelength (785 nm) while the 28 μm core is highly multi-mode (MM) at the excitation as well as the Raman-shifted signal wavelengths. The effective diameter encompassing the excitation and collection cores is 47 μm and the outer diameter of the fibre itself is 125 μm. The asymmetric dual core arrangement was used to spatially separate the collection path from the excitation path where the intense Raman background is generated. A commercial step-index multimode (MM) fibre with a 50 μm Ge:doped core and an outer diameter of 125 μm was subsequently spliced to the dual-core fibre. The loss across the splice in the proximal to distal direction was found to be < 0.5 dB, when 785 nm coherent light was injected into the 28 μm core. The measured loss in the reverse direction was consistent with that expected due to the geometric difference between the core dimensions. The length of the spliced MM fibre which formed the optrode was ~ 0.5 mm, measured from the splice plane making it ~0.01 % of the total length of the dual-core fibre. The short length was essential in order to minimise the Raman background generated within its core. However, its length was adequate to ensure optimal spatial overlap between the modes exiting the end-facet for both SM and MM injection of 785 nm light at the proximal end. The spliced MM section was packaged in a custom fused silica end-cap, which was fabricated using ultrafast laser inscription and selective wet etching [16]. This ensured mechanical robustness of the optrode during transbronchial passes performed in practical clinical application. A 20 μm^3 recess was machined (using 120fs pulses of 800 nm light at 5 kHz) at the facet of the 50 μm MM core to prevent nanoshell loss during transbronchial passes. Finally, the entire fibre was packaged inside a 2.5 m long biocompatible polymer tube (PEEK) with an outer diameter of 1.5 mm, which is well below the inner diameter of the working channel of most standard bronchoscopes. A 1.5 μL suspension of para-mercaptobenzoic acid (p-MBA) [17] functionalised 150 nm Au nanoshells (Nanospectra Biosciences) was pipetted on the end-prepared facet of the optrode, which was pre-treated with poly-L lysine (0.1 mg/mL) to enhance the adherence of nanoshells to the machined silica surface. The large surface area

of the silica distal end-cap allowed the pipetted droplet to evaporate at ambient temperature within a few minutes. The end-facet was further encapsulated using a permeable sol-gel layer to minimise contact-induced nanoshell loss.

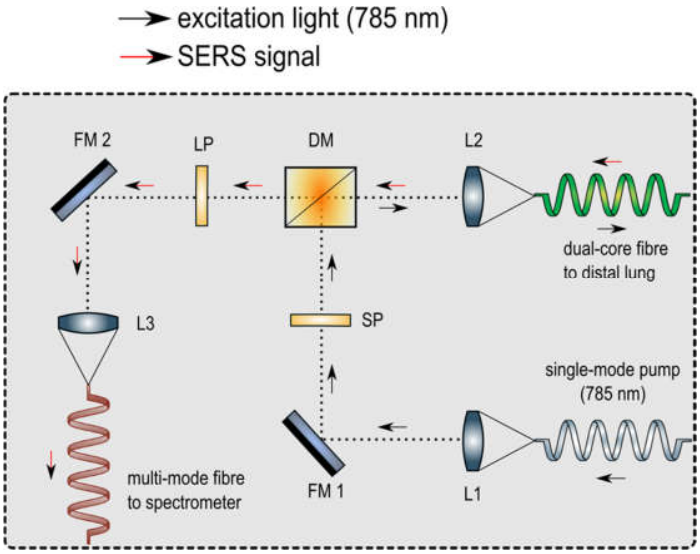

Figure 3. Schematic showing the proximal end optical instrument (First published in [1]).

At the proximal end of the device, a free-space optical instrument was used to input couple the excitation light into the SM core of the dual-core fibre and output couple the Raman-shifted signal light to the spectrometer. The mode at 785 nm from a SM fibre (Thorlabs, 780-HP) was imaged at unit magnification using aspheric lenses (L1 & L2) onto the SM excitation core. The signal light from the MM collection core was output coupled using lens L2 and imaged at unit magnification using the lens L3 and a kinematic adjuster (FM 2) onto the step-index 25 μm core of a MM patch-cable, after passing through a dichroic (DM) enabling fibre-Raman background suppressed operation of the sensing probe. A short-pass filter (SP) was placed in the input beam path to filter any long wavelength amplified spontaneous emission from the laser source. A long-pass filter (LP) was placed in the output beam path to prevent 785 nm light from being acquired by the spectrometer. The output of the patch-cable was directly coupled to the spectrometer (Ocean Optics, QE Pro) through a 25 μm slit.

3. On-bench probe characterisation

We used a distal-end power output of ~ 0.4 mW for both the calibration and EVLP experiments. Spectra obtained using the probe under normal and background-suppressed modes of operation showed an ~100-fold fibre-Raman background suppression using the instrument. The characteristic spectral features of p-MBA were almost completely identical to that recorded using gold-coated slides [18]. The pH-dependent variation in the p-MBA SERS spectrum obtained using the packaged miniaturised fibre-optic probe was assessed using buffers with pH ranging from 4.0 to 9.0. A total of 21 buffer solutions were prepared within the physiologically relevant range of pH 6.0 to 8.0. 165 SERS spectra were acquired and averaged in 5 non-sequential replicate measurements. The order of measurement was randomised within each replicate in order to avoid systematic error. The raw data were computationally processed using algorithms developed to adaptively "learn" and eliminate contributions from any residual background from pH driven changes in the spectrum. The post-processed spectra were subsequently assessed for variations in the ratio between the area under the curve (AUC) within a 50 cm-1 (±25 cm-1) window centred at Raman shifts of 1380 cm^{-1} and 1700 cm^{-1}, the spectral features most

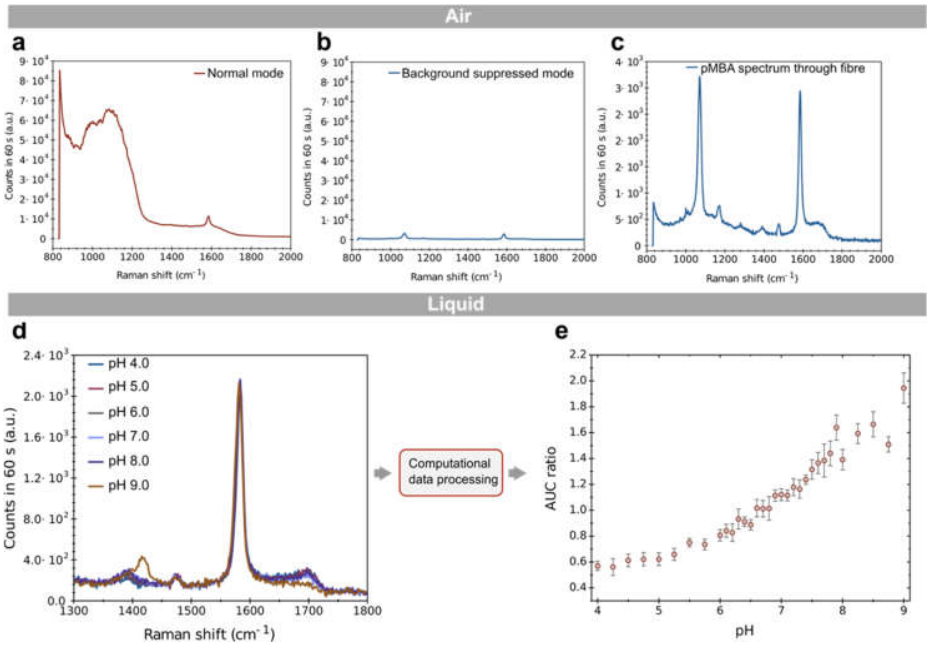

Figure 4. Background suppressed p-MBA SERS spectrum and its characteristics with respect to change in pH, observed using the packaged fibre-optic optrode. (a)Spectrum acquired when the MM core was used for both excitation and collection (normal mode). (b) Spectrum acquired when the SM and MM cores were used for excitation and collection respectively (background suppressed mode). (c) Characteristic p-MBA SERS spectrum acquired using the fibre-optic optrode. (d) Spectrum from 1300 cm^{-1} to 1800 cm^{-1} showing pH sensitive response in the vicinity of 1380 cm^{-1} and 1700 cm^{-1}. (e) Variation of the area under the curve (AUC) ratio with respect to pH in the range 4.0 – 9.0. (First published in [1]).

sensitive to pH variation [19]. A well-defined and consistent variation within the physiologically relevant pH range was observed. The intrinsic measurement accuracy of the probe between pH 6.4 and pH 7.4 was found to be 0.07 pH unit.

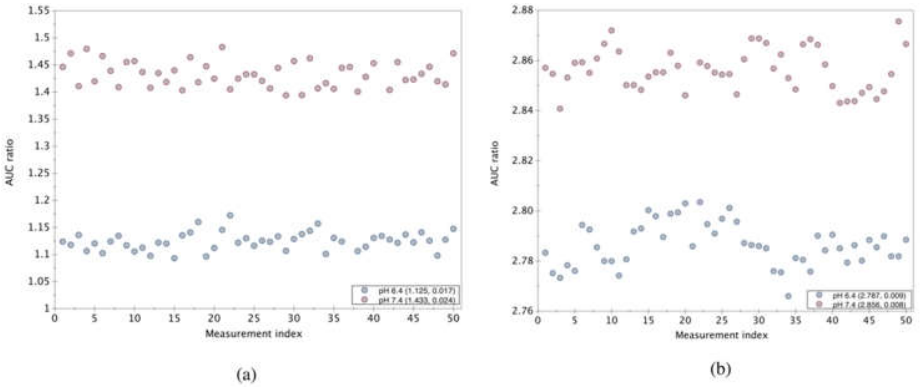

Figure 5. The measurement accuracy of the fibre-optic probe in the case of background-suppressed (a) and normal (b) mode of operation. Measurements were acquired using buffer solutions of pH 6.4 and pH 7.4 (First published in [1]).

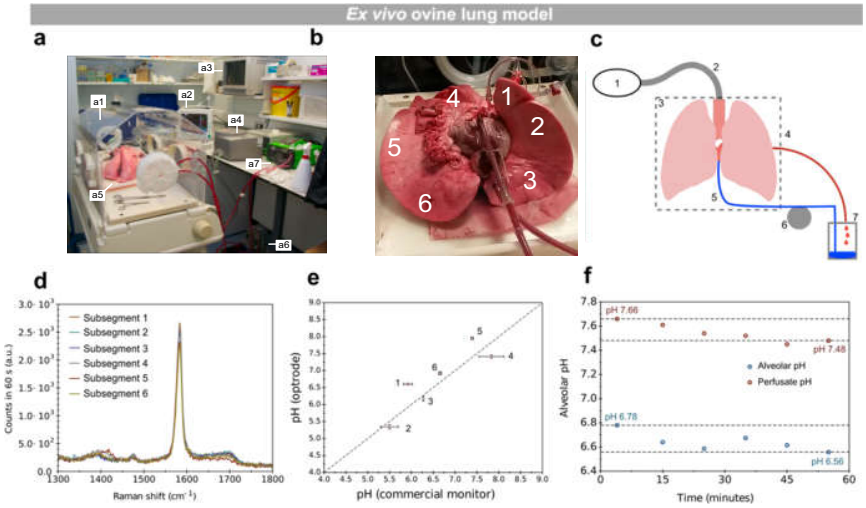

Figure 6. Alveolar space pH measured using the fibre-optic optrode in an ex vivo ovine lung model. **(a)** Photograph of the ex vivo ovine lung perfusion and ventilation set-up used for the experiment. **a1**: Incubator **a2**: Physiology monitor **a3**: Bronchoscopy screen **a4**: Ventilator and closed breathing circuit **a5**: Ventilated ovine lung **a6**: Water bath and perfusate circuit **a7**: Roller pump. **(b)** Arrangement of anatomically distinct pulmonary lobes and segments of the ovine lung. The numbers represent the six subsegments interrogated using the fibre-optic probe **(c)** Illustration showing the perfusion and ventilation circuits used in the experiment. 1: Ventilator, 2: Breathing circuit, 3: Incubator and humidifier, 4: Left atrial cannula, 5: Pulmonary artery cannula, 6: Roller pump, 7: Reservoir **(d)** p-MBA spectrum between 1300 cm^{-1} and 1800 cm^{-1}, obtained from the sequential interrogation of the six distal subsegments shown in (b). **(e)** The alveolar pH measured using the fibre-optic optrode for the six subsegments (y-axis). The x-axis represents the pH measured using the commercial pH monitor at the incised locations for each subsegment. The numbers indicate the order in which the instilled subsegments were interrogated using the fibre-optic optrode. **(f)** Alveolar pH variation as a function of time in an ex vivo ovine lung model with ceased ventilation (t = 0) measured using the fibre-optic optrode. The variation of perfusate pH with time measured using a commercial pH probe is also shown. (First published in [1]).

4. Experimental validation in an *ex vivo* lung model

We used an *ex vivo* perfused and ventilated ovine lung model to test and validate the probe's performance. The validation was performed using two distinct experiments as discussed in the sections below.

4.1. *Multi-site interrogation*

Serial alveolar pH measurements were performed in a human-size lung model in distinct bronchopulmonary segments. Six distal sub-segments in the lung were instilled with 10 mL of buffer solutions within the pH range of 2.0 to 12.0. As the instilled solutions could access the perfused vasculature and affect other sub-segments, the lung was not perfused for the duration of this experi ment. Thus 6 independent pH measurements to be acquired without the risk of cross-contamination. After a 30-minute interval to allow for self-buffering, the sub-segments were sequentially interrogated using the packaged fibre-optic probe and the spectra were recorded with an integration time of 60 s using 0.2 mW

of 785 nm coherent excitation light. The probe was inserted through the working channel of a standard flexible bronchoscope (Olympus) and navigated through the bronchial tree prior to performing a transbronchial pass into the alveolar space of each sub-segment. The location of the probe at the distal end was marked on the exterior of the lung and spectral measurements were performed in three sequential repetitions. At the end of the experiment, three incisions were made within the vicinity (~ 5 mm) of each marked location and a commercial wide-bore tissue pH monitor (Mettler Toledo) was used to measure the pH in the respective sub-segments. The optical measurements were objectively validated at multiple closely-spaced incisions due to the large difference in bore diameter between the two probes, which led to the inability to accurately determine the exact location in the alveoli where the fibre-optic interrogation was performed through the respiratory tract. The alveolar pH evaluated from the spectral AUC ratio were found to be in good agreement with the pH measured using the commercial probe. Each sub-segment showed the expected disparity in measured pH from that of the pre-instilled fluid due to self-buffering. In the case of 3 sub-segments (1, 2 and 4), the pH measured using the commercial probe revealed notable variations (>0.8 pH unit) across a short spatial measurement range (<1 cm), which caused an apparent lowering in correlation between the respective validation measurements. This can be attributed to the fact that for these sub-segments, the tip of the wide-bore commercial probe could not be precisely co-located with the miniature fibre-optic probe.

4.2. *Temporal interrogation of a single site under ventilation arrest*

Using the model, we further conducted an experiment to demonstrate the sensitivity of the fibre-optic probe to temporal variations in the distal lung pH. The probe was positioned at the distal end of a single sub-segment in the distal lung. The lung was not ventilated but perfusion was maintained throughout the duration of the experiment. Over 60 minutes, samples of perfused blood were extracted at 10-minute intervals and the pH measured with a commercial pH probe. SERS spectra from the alveolar space were concomitantly acquired using the fibre-optic probe. The temporal variation in alveolar pH were found to be consistent with that of the perfused blood, with both measurements showing the expected correlated reduction in pH when ventilation was stopped.

5. Conclusion

The miniaturised fibre-optic pH sensing probe discussed here offers a platform technology that can potentially be multiplexed with other SERS reporters. This will enable the concurrent *in vivo* and *in situ* monitoring of additional physiological parameters in the alveolar space such as oxygen tension and glucose levels. The factor of ~100-fold improvement in signal to fibre background means that in such measurement schemes, the measurement is no longer limited by the Raman contribution from the fibre itself. Importantly, this technological advance will be significant in the case of SERS molecular reporters with signal features at lower Raman shift, where the silica background is orders of magnitude larger. We envisage that with ongoing improvements in SERS sensitivity and instrument performance, this technology has the potential to complement existing endoscopic procedures and generate new physiological markers of lung disease.

Funding

The authors gratefully acknowledge the UK Engineering and Physical Sciences Research Council (EP/K03197X/1) for funding this work.

References

[1] D. Choudhury, M. G. Tanner, S. McAughtrie, F. Yu, B. Mills, T. R. Choudhary, S. Seth, T. H. Craven, J. M. Stone, I. K. Mati, C. J. Campbell, M. Bradley, C. K. I. Williams, K. Dhaliwal, T. A. Birks, and R. R. Thomson, "Endoscopic sensing of alveolar pH," Biomed. Opt. Express **8**, 243-259 (2017).

[2] A. Ricciardi, A. Crescitelli, P. Vaiano, G. Quero, M. Consales, M. Pisco, E. Esposito, and A. Cusano, "Lab-on-fiber technology: a new vision for chemical and biological sensing," Analyst

140, 8068–8079 (2015).

[3] P. R. Stoddart and D. J. White, "Optical fibre SERS sensors," Anal Bioanal Chem **394**, 1761–1774 (2009).

[4] E. J. Smythe, M. D. Dickey, J. Bao, G. M. Whitesides, and F. Capasso, "Optical Antenna Arrays on a Fiber Facet for in SituSurface-Enhanced Raman Scattering Detection," Nano Lett. **9**, 1132–1138 (2009).

[5] D. I. Ellis, D. P. Cowcher, L. Ashton, S. O'Hagan, and R. Goodacre, "Illuminating disease and enlightening biomedicine: Raman spectroscopy as a diagnostic tool," Analyst **138**, 3871–3884 (2013).

[6] J. T. Motz, M. Hunter, L. H. Galindo, J. A. Gardecki, J. R. Kramer, R. R. Dasari, and M. S. Feld, "Optical Fiber Probe for Biomedical Raman Spectroscopy," Appl. Opt. **43**, 542–554 (2004).

[7] J. T. Motz, S. J. Gandhi, O. R. Scepanovic, A. S. Haka, J. R. Kramer, R. R. Dasari, and M. S. Feld, "Real-time Raman system for in vivo disease diagnosis," J. Biomed. Opt. **10**, 031113 (2005).

[8] Y. Komachi, H. Sato, K. Aizawa, and H. Tashiro, "Micro-optical fiber probe for use in an intravascular Raman endoscope," Appl. Opt. **44**, 4722–4732 (2005).

[9] S. Dochow, I. Latka, M. Becker, R. Spittel, J. Kobelke, K. Schuster, A. Graf, S. Brückner, S. Unger, M. Rothhardt, B. Dietzek, C. Krafft, and J. Popp, "Multicore fiber with integrated fiber Bragg gratings for background-free Raman sensing," Optics Express **20**, 20156–20169 (2012).

[10] B. B. Praveen, C. Steuwe, M. Mazilu, K. Dholakia, and S. Mahajan, "Wavelength modulated surface enhanced (resonance) Raman scattering for background-free detection," Analyst **138**, 2816–2820 (2013).

[11] H. Yan, C. Gu, C. Yang, J. Liu, G. Jin, J. Zhang, L. Hou, and Y. Yao, "Hollow core photonic crystal fiber surface-enhanced Raman probe," Appl. Phys. Lett. **89**, 204101 (2006).

[12] X. Yang, C. Shi, R. Newhouse, J. Z. Zhang, and C. Gu, "Hollow-Core Photonic Crystal Fibers for Surface-Enhanced Raman Scattering Probes," International Journal of Optics **2011**, 1–11 (2011).

[13] D. Pristinski and H. Du, "Solid-core photonic crystal fiber as a Raman spectroscopy platform with a silica core as an internal reference," Optics Letters **31**, 3246 (2006).

[14] [14] G. F. S. Andrade, M. Fan, and A. G. Brolo, "Multilayer silver nanoparticles-modified optical fiber tip for high performance SERS remote sensing," Biosensors and Bioelectronics **25**, 2270–2275 (2010).

[15] J. C. Knight, "Photonic crystal fibres," Nature **424**, 847–851 (2003).

[16] D. Choudhury, J. R. Macdonald, and A. K. Kar, "Ultrafast laser inscription: perspectives on future integrated applications," Laser & Photon. Rev. **8**, 827–846 (2014).

[17] S. W. Bishnoi, C. J. Rozell, C. S. Levin, M. K. Gheith, B. R. Johnson, D. H. Johnson, and N. J. Halas, "All-Optical Nanoscale pH Meter," Nano Lett. **6**, 1687–1692 (2006).

[18] Y. Liu, H. Yuan, A. M. Fales, and T. Vo-Dinh, "pH-sensing nanostar probe using surface-enhanced Raman scattering (SERS): theoretical and experimental studies," J. Raman Spectrosc. **44**, 980–986 (2013).

[19] A. Jaworska, L. E. Jamieson, K. Malek, C. J. Campbell, J. Choo, S. Chlopicki, and M. Baranska, "SERS-based monitoring of the intracellular pH in endothelial cells: the influence of the extracellular environment and tumour necrosis factor-α," Analyst **140**, 2321–2329 (2015).